19th International Conference
ENGINEERING MECHANICS 2013
Svratka, Czech Republic, May 13 – 16, 2013

Identification of damping parameters of bladed disks

J. Kellner, V. Zeman, J. Šašek, Z. Kubín [1]

Abstract: *Regarding steam turbine blade vibrations, damping of blades as well as whole bladed disk vibrations are one of the most important parameters in terms of steam turbine operation. Values of the damping parameters depend on properties of material used for blades and disc as well as on geometric parameters of blade shroud contact areas with friction elements. The in-house made software enables fast parametric optimization using a multi-criteria function, for example angle of contact planes or mass of friction elements. The real bladed disk was excited in vacuum machine to provide material and construction damping. The measured modal properties and damping parameters identification are used for model correction as well as for detailed meshed model in commercial software.*

Keywords: ***steam turbine blades, damping, friction element, parameter identification.***

1. Introduction

The need for higher efficiency leads to thinner blades profile on one hand but the requirement of higher stage power output with different operation points leads to higher bending stress in blade on other hand. This higher stress in blade is resulting in smaller dynamic load which can be applied on blades. One of the most usual approaches to the suppression of the undesirable blade vibrations is application of the friction elements and connection to continuous coupled set of blades. In order to increase stiffness and damping of turbine blades a new type of shrouds with friction contacts was developed. However the effect of the friction contact cannot be determined during design process without deeper knowledge of this type friction and without identification of other damping parameters.

That is why the first goal of this article is damping identification of new type of shrouded blades depending on excitation amplitude. The damping phenomena is very complex. Damping in real bladed disk usually includes material damping, ”unwanted” root construction damping, friction damping and other issues, for example the air resistance. In order to uncover all aspects of the real blade damping, we will proceed step by step.

From measurement point of view, the good agreement will be presented between the damping ratio of beams specimens and free blades as well as the issues of identification of coupled blades damping. Damping dependence on the amplitude of blade vibration or on the number of nodal diameters will also be discussed.

In theoretical part of this article, the FEM results of in-house code are compared with commercial software as well as with measurement. For real-time design process, the methodology for quick and reliable model creation is included. The methodology involves modal condensation in the sense of degree of freedom reduction. This part is important for damping element

[1] Ing. Josef Kellner, Ph.D., Ing. Jakub Šašek, Ph.D., Prof. Ing. Vladimír Zeman, DrSc.,Ing. Zdeněk Kubín, Faculty of Applied Sciences, Univerzitní 22, 326 00 Pilsen, e-mail kkenny@seznam.cz

parameters designing - as discussed in Hajžman et al., (2013) - the shape, position and other geometric properties have different influence on optimization parameters from the point of view of dynamic response in different resonance states.

2. Geometric specification

Firstly, the experimental (real bladed) disk was made with 56 high pressure blades. After first measurement with free standing blades, the friction elements were placed between shrouds (i.e. the tops of blades) to increase the total damping as well as stiffness of system (fig. 1). There are two contact areas in points A_i, B_i with different slope angle, that's why there are two different contacts in the sense of behavior.

The bladed disk is placed in vacuum chamber to eliminate air damping. The blades are connected with disk by so called T-root, see fig. 2. There are two radial and two axial contacts. Due to centrifugal force, the relative movement between blade root and disk groove can be assume as non-sliding with regard to calculation of natural frequencies and mode shapes. That's why this connection is in presented methodology modelled as rigid.

The "construction" damping in root is often unwanted for this type of blades - it can cause fretting cracks and it can damage the contact areas in root. For steam turbine blades there are small relative deformations (relative displacements) in the root part contact areas (fig. 2). The underplatform dampers, mainly used in aircraft engines, are inefficient for steam blades. But this measured "construction" damping is added to material damping in the mathematical model.

The blades airfoil was change to slim beam after several measurement, see below.

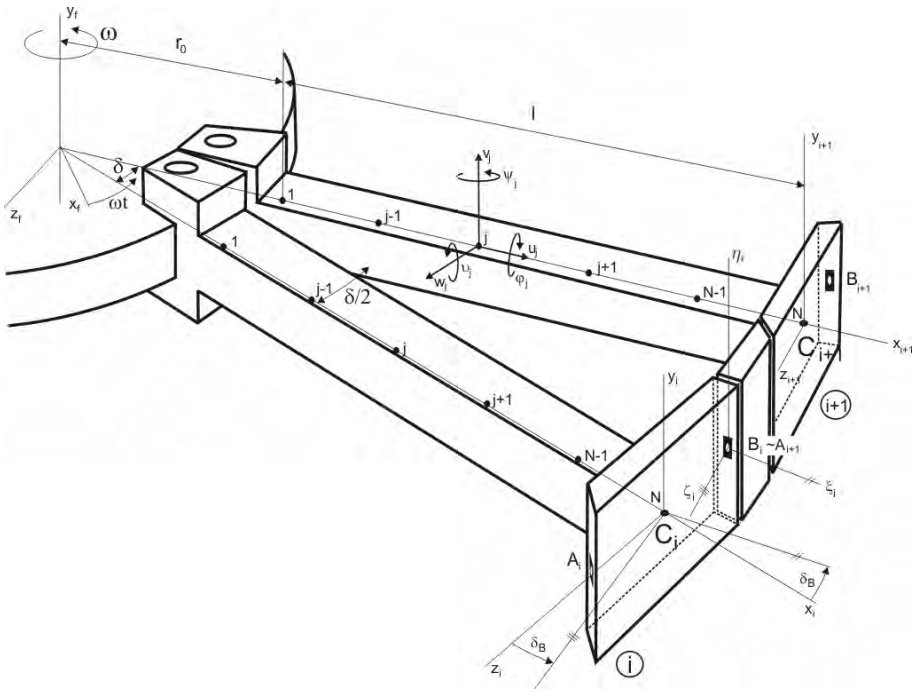

Figure 1: Scheme of two adjacent blades and damping element.

3. Measured material damping

The measurement of damping is very sensitive on many aspects: the roughness of contact areas, size of real contact area, type of material and other aspects discussed above. The first step to precise the results is the knowledge of material damping.

Firstly, the rectangular beams were made from same material as the blades. The individual beams were clamped at 2 ton cube by force approximately 500 kN between wedges, that is why zero initial conditions were assured. Then an accelerometer was installed at the top of the beam and a strain gauge was placed on the bottom of the beam. The impulse hammer or statically deflection of beam top as initial condition were used for measurement of material damping (fig. 3).

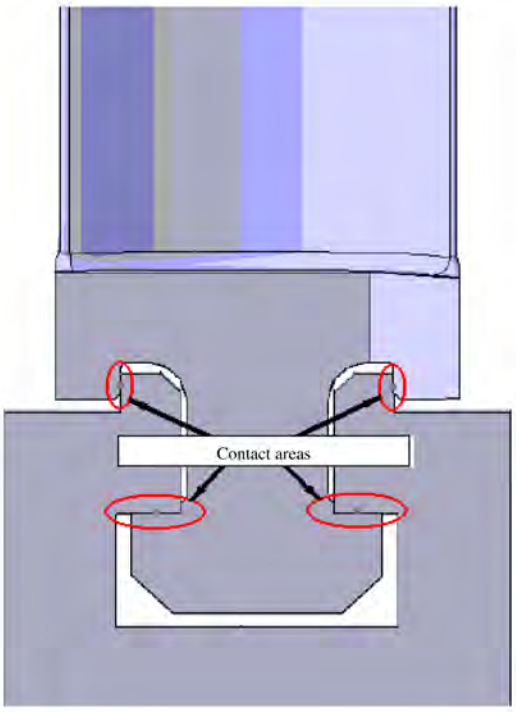

Figure 2: Scheme of T-root connection.

Figure 3: Fixed beam for material damping measurement.

The frequency as well as the geometrical shape of beam were close to the inspected blades. In fig. 4 there is the material damping dependence on the initial bending stress in the bottom (i.e. the initial displacement of the beam top). The material damping was evaluated for two directions of initial statically deflection - the red and green curves express damping ratio of the first two mode shapes.

From this measurement it can be seen, that the material damping is nonlinear dependent on initial stress (although this stress is linear dependent on initial deflection for elastic deformation). The bending stress for real blades is in relatively low range. More details of measurement for various types of blade couplings are in paper Kubín et al., (2013). Blue points demonstrate at the fig. 4 the damping ratio for free standing blades in the bladed disk (3000 rpm), see next sections.

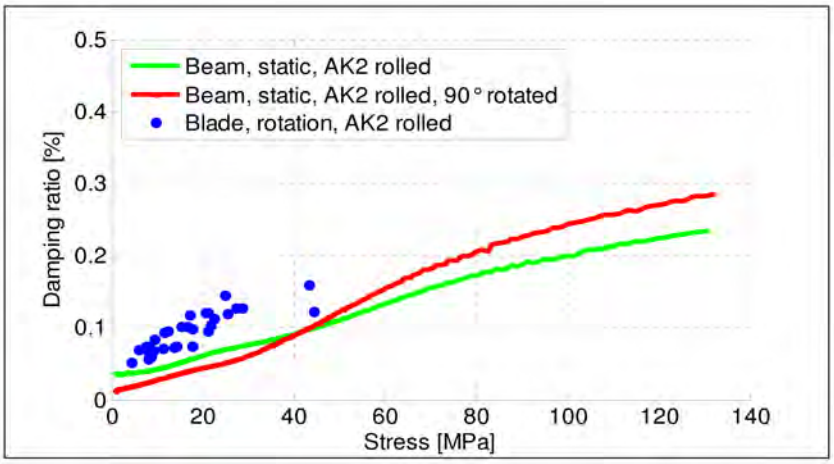

Figure 4: Damping ratio of free standing blades under rotation in comparison with material damping ratio of beam cut out of the identical material.

4. Blade model and verification

The single blades are modelled as one dimensional continuum linked with rigid shroud body in its centre of gravity of last blade profile - fig. 1. The mathematical model of the uncoupled blade i with shroud in configuration space of its blade node displacements (in the direction of rotating axes x_i, y_i, z_i and of small angular displacements of the blade cross sections)

$$\boldsymbol{q}_{B,i} = [\ldots, u_j, v_j, w_j, \varphi_j, \vartheta_j, \psi_j, \ldots]^T_{B,i} \in \mathcal{R}^{n_B},\ i = 1, 2, \ldots, r; j = 1, 2, \ldots, N \qquad (1)$$

has the form (Kellner and Zeman (2006); Kellner (2009))

$$\boldsymbol{M}_B \ddot{\boldsymbol{q}}_{B,i}(t) + \omega \boldsymbol{G}_B \dot{\boldsymbol{q}}_{B,i}(t) + \left(\boldsymbol{K}_{sB} + \omega^2 \boldsymbol{K}_{\omega B} - \omega^2 \boldsymbol{K}_{dB}\right) \boldsymbol{q}_{B,i}(t) = \omega^2 \boldsymbol{f}_B\,, \qquad (2)$$

where $\boldsymbol{M}_B$, $\boldsymbol{K}_{sB}$ and $\boldsymbol{K}_{dB}$ are symmetric mass, static stiffness and dynamic softening matrices, skew-symmetric matrix $\boldsymbol{G}_B$ expresses gyroscopic effects , matrix $\boldsymbol{K}_{\omega,B}$ expresses a centrifugal blade stiffening and $\omega^2 \boldsymbol{f}_B$ is force vector of centrifugal load.

The blade model created in MATLAB (36 degree of freedom = DOF) was compared with FE model in ANSYS (15 000 DOF) and with measurement, see tab. 1. The first natural frequency of blade in MATLAB is close to ANSYS, both models are 30 Hz far from measurement. This reason can be in different boundary conditions. The measurement was done in hydraulic press, where the blade is fixed in root, but the connection is not so ideal as in FE models. In tangential direction it is less rigid. In ANSYS, the blade was fixed in the platform (the top of the blade root) and in MATLAB it was fixed in the first node of FE model. Although this is very rigid fixation the FE models are similar for the first frequency. The difference between FE models as well as measurement increase but it is in range $\pm 0.9_{\%}$. For MATLAB accuracy verification the model with 96 DOF was done, but it can be seen that there is no significant difference - 3^{rd} and 4^{th} column in tab. 1.

In the right part of the tab. 1 there are natural frequencies in rotating state. The change of stiffness due to centrifugal forces is same for both FE models (it can not be measured in hydraulic press). It can be assumed that the MATLAB model of one blade has sufficient accuracy.

Table 1: Natural frequencies of blade - measurement and FE models

Natural frequencies of fixed blade [Hz]					
0 rpm				3000 rpm	
Measured	ANSYS	MATLAB 5 elements	MATLAB 15 elements	ANSYS	MATLAB 5 elements
Fixed on root	Fixed on platform	Fixed on airfoil	Fixed on airfoil	Fixed on platform	Fixed on airfoil
390	420,03	419,07	419,07	435,1	432,55
842	848,07	860,60	860,60	854	866,11
1624	1600	1455,81	1455,80	1600	1455,57

5. The blade rim with friction elements in shroud – contact stiffness

This model, detailed described in Zeman et al., (2009) respects both contact stiffness between blade i and friction element and between friction element and following blade $i+1$. These contact stiffnesses are defined by contact stiffness matrix between corresponding blades i and $i+1$

$$\mathbf{K}_C^{(X)} = diag\,(0 \quad 0 \quad k_\zeta \quad k_{\xi\xi} \quad k_{\eta\eta} \quad 0)_{\xi_i,\eta_i,\zeta_i}\,, X = A, B, \tag{3}$$

expressing the constraint for the circumferential displacement and two rotations by means of contact stiffness k_ζ in normal direction to contact area $\xi_i\eta_i$ and two flexural stiffnesses $k_{\xi\xi},\ k_{\eta\eta}$.

This contact stiffness matrix is expressed in local contact coordinate system ξ_i, η_i, ζ_i placed in central contact point B_i, respectively A_i of the i-th blade shroud. The coupling (deformation) energy between two adjacent blades i and $i+1$ (see fig. 1) is, in this contact coordinate system, expressed as

$$E_C^{i,i+1} = \frac{1}{2}\left(\boldsymbol{q}_{B_i} - \boldsymbol{q}_{E_i}\right)^T \mathbf{K}_C^{(B)} \left(\boldsymbol{q}_{B_i} - \boldsymbol{q}_{E_i}\right) + \frac{1}{2}\left(\boldsymbol{q}_{E_i} - \boldsymbol{q}_{A_{i+1}}\right)^T \mathbf{K}_C^{(A)} \left(\boldsymbol{q}_{E_i} - \boldsymbol{q}_{A_{i+1}}\right), \tag{4}$$

where $\boldsymbol{q}_{B_i}, \boldsymbol{q}_{A_{i+1}}$ are vector of blade i displacements in point B_i and vector blade $i+1$ displacements in pointA_{i+1} expressed in coordinate system ξ_i, η_i, ζ_i. The vector $\boldsymbol{q}_{E_i}$ is vector of friction element displacements. The difference between $\boldsymbol{q}_{B_i} - \boldsymbol{q}_{E_i}$ and $\boldsymbol{q}_{E_i} - \boldsymbol{q}_{A_{i+1}}$ represents the relative motion of two contact areas between two adjacent blades i and $i+1$.

The translation of blade local coordinate systems from point C_i to point B_i and from point C_{i+1} to point A_{i+1} is expressed by translation matrices

$$\boldsymbol{R}_X^T = \begin{bmatrix} 0 & z_X & -y_X \\ -z_X & 0 & x_X \\ y_X & -x_X & 0 \end{bmatrix}, \quad X = A_{i+1}, B_i. \tag{5}$$

The translated local coordinate system is then rotated so, that the contact coordinate axis ξ_i is the radial according to bladed disk axis of rotation y_f.

The vector of displacements in point B_i in the corresponding contact coordinate system is

$$\boldsymbol{q}_{B_i\ \xi_i,\eta_i,\zeta_i} = \begin{bmatrix} u_{B_i} \\ v_{B_i} \\ w_{B_i} \\ \varphi_{B_i} \\ \vartheta_{B_i} \\ \psi_{B_i} \end{bmatrix}_{\xi_i,\eta_i,\zeta_i} = \left[\begin{array}{c|c} \boldsymbol{\tau}_B & \mathbf{0} \\ \hline \mathbf{0} & \boldsymbol{\tau}_B \end{array}\right] \begin{bmatrix} u_{B_i} \\ v_{B_i} \\ w_{B_i} \\ \varphi_{B_i} \\ \vartheta_{B_i} \\ \psi_{B_i} \end{bmatrix}_{x_i,z_i,y_i} \begin{matrix} \left.\begin{matrix} \\ \\ \end{matrix}\right\} \mathbf{u}_{B_i} \\ \left.\begin{matrix} \\ \\ \\ \end{matrix}\right\} \boldsymbol{\varphi}_{B_i} \end{matrix} \Bigg\} \boldsymbol{q}_{B_i\ x_i,y_i,z_i}, \tag{6}$$

where the rotation matrix $\boldsymbol{\tau}_B$ between coordinate systems is specified by angle δ_B between radial axis x_i of blade passing through point C_i and radial axis ξ_i passing through point B_i

$$\boldsymbol{\tau}_B = \begin{bmatrix} \cos\delta_B & 0 & -\sin\delta_B \\ 0 & 1 & 0 \\ \sin\delta_B & 0 & \cos\delta_B \end{bmatrix}. \tag{7}$$

Analogously the vector of displacements of point A_{i+1} in this contact coordinate system is defined as

$$\boldsymbol{q}_{A_{i+1}\ \xi_i,\eta_i,\zeta_i} = \begin{bmatrix} \boldsymbol{\tau}_A & \mathbf{0} \\ \mathbf{0} & \boldsymbol{\tau}_A \end{bmatrix} \boldsymbol{q}_{A_{i+1}\ x_{i+1},y_{i+1},z_{i+1}}, \tag{8}$$

where

$$\boldsymbol{\tau}_A = \begin{bmatrix} \cos\delta_A & 0 & \sin\delta_A \\ 0 & 1 & 0 \\ -\sin\delta_A & 0 & \cos\delta_A \end{bmatrix}. \tag{9}$$

The vector of blade i displacements in point B_i in coordinate system x_i, y_i, z_i is defined by generalized displacements of point C_i and by matrix of translation $\boldsymbol{R}_B$

$$\boldsymbol{q}_{B_i\ x_i,y_i,z_i} = \begin{bmatrix} \boldsymbol{u}_{B_i} \\ \boldsymbol{\varphi}_{B_i} \end{bmatrix}_{x_i,y_i,z_i} = \begin{bmatrix} \boldsymbol{E} & \boldsymbol{R}_B^T \\ \mathbf{0} & \boldsymbol{E} \end{bmatrix} \begin{bmatrix} \boldsymbol{u}_{C_i} \\ \boldsymbol{\varphi}_{C_i} \end{bmatrix}_{x_i,y_i,z_i} = \begin{bmatrix} \boldsymbol{E} & \boldsymbol{R}_B^T \\ \mathbf{0} & \boldsymbol{E} \end{bmatrix} \boldsymbol{q}_{C_i}. \tag{10}$$

According to (6) this vector in the contact coordinate system ξ_i, η_i, ζ_i has the form

$$\boldsymbol{q}_{B_i\ \xi_i,\eta_i,\zeta_i} = \underbrace{\begin{bmatrix} \boldsymbol{\tau_B} & \mathbf{0} \\ \mathbf{0} & \boldsymbol{\tau}_B \end{bmatrix} \begin{bmatrix} \boldsymbol{E} & \boldsymbol{R}_B^T \\ \mathbf{0} & \boldsymbol{E} \end{bmatrix}}_{\boldsymbol{T}_B} \boldsymbol{q}_{C_i\ x_i,y_i,z_i}. \tag{11}$$

Analogously, the vector of blade $i+1$ displacements in point A_{i+1} in the contact coordinate system ξ_i, η_i, ζ_i is expressed as

$$\boldsymbol{q}_{A_{i+1}\ \xi_i,\eta_i,\zeta_i} = \underbrace{\begin{bmatrix} \boldsymbol{\tau_A} & \mathbf{0} \\ \mathbf{0} & \boldsymbol{\tau}_A \end{bmatrix} \begin{bmatrix} \boldsymbol{E} & \boldsymbol{R}_A^T \\ \mathbf{0} & \boldsymbol{E} \end{bmatrix}}_{\boldsymbol{T}_A} \boldsymbol{q}_{C_{i+1}\ x_{i+1},y_{i+1},z_{i+1}}. \tag{12}$$

We can now express the coupling energy, defined in (4)by means of generalized coordinates of i-th and $i+1$-th blades in the form

$$E_C^{i,i+1} = \frac{1}{2}\left(\boldsymbol{T}_B\boldsymbol{q}_{C_i} - \boldsymbol{T}_{E,B}\boldsymbol{q}_{E_i}\right)^T \mathbf{K}_C^{(B)} \left(\boldsymbol{T}_B\boldsymbol{q}_{C_i} - \boldsymbol{T}_{E,B}\boldsymbol{q}_{E_i}\right) + \frac{1}{2}\left(\boldsymbol{T}_{E,A}\boldsymbol{q}_{E_i} - \boldsymbol{T}_A\boldsymbol{q}_{A_{i+1}}\right)^T \mathbf{K}_C^{(A)} \left(\boldsymbol{T}_{E,A}\boldsymbol{q}_{E_i} - \boldsymbol{T}_A\boldsymbol{q}_{A_{i+1}}\right). \tag{13}$$

After multiplying the previous equation and from identity $\frac{\partial E_C^{i,i+1}}{\partial \boldsymbol{q}_R} = \boldsymbol{K}_{C_i}^{(R)} \boldsymbol{q}_R$, where $\boldsymbol{q}_R$ is vector of blade rim displacements, we obtain the stiffness matrix of coupling $\mathbf{K}_{C_i}^{(R)}$ between two adjacent blades i and $i+1$.

By summation of all these individual matrices for all contact areas we obtain the global contact stiffness matrix connecting all the blades together into a blade rim, whose equation of motion is

$$\boldsymbol{M}_R \ddot{\boldsymbol{q}}_R(t) + \omega \boldsymbol{G}_R \dot{\boldsymbol{q}}_R(t) + \left(\boldsymbol{K}_{sR} + \boldsymbol{K}_C^{(R)} + \omega^2 \boldsymbol{K}_{\omega R} - \omega^2 \boldsymbol{K}_{dR} \right) \boldsymbol{q}_R(t) = \omega^2 \boldsymbol{f}_R \,, \tag{14}$$

where all matrices (except $\boldsymbol{K}_C^{(R)}$) are block-diagonal in the form

$$\boldsymbol{X}_R = diag\left(\boldsymbol{X}_B,\, \boldsymbol{X}_B,\, \ldots,\, \boldsymbol{X}_B\right), \quad \boldsymbol{X} = \boldsymbol{M}, \boldsymbol{G}, \boldsymbol{K}_s, \boldsymbol{M}_d, \boldsymbol{K}_\omega, \boldsymbol{f}. \tag{15}$$

6. Modelling of the friction element

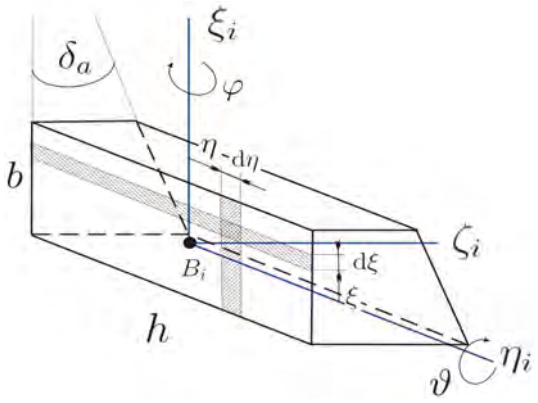

Figure 5: Scheme of the friction element.

The contact stiffness matrix $\boldsymbol{K}_C^{(B)}$ between friction element and one blade shroud defined in (3), depends on geometric and material characteristics of friction element. The normal force in the contact is

$$N_0 = \frac{m_T r \omega^2}{\tan \delta_i}, \; i = \alpha, \beta, \tag{16}$$

where m_T is the friction element mass, δ_i is angle of the corresponding contact area, $\omega = \frac{\pi n}{30}$ is the angular velocity and r is radius of friction element centre of gravity. The contact stress is

$$\sigma_{[MPa]} = \frac{N_{0\,[N]}}{A_{ef\,[mm^2]}}, \quad A_{ef} = \overbrace{h\gamma_h}^{h_{ef}} \overbrace{b\gamma_b}^{b_{ef}} .10^6 \tag{17}$$

where h is axial and b is radial friction element proportions and A_{ef} is the effective contact area (see fig. 5), defined by real size of contact area, i.e. the high h multiply by coefficient γ_h etc. The contact stiffness figuring in the matrix $\mathbf{K}_C^{(B)}$ in 3 can be determined on the basis of the contact stress. For more details see Kellner et al., (2010).

7. The mathematical modelling of the disk

Disk is clamped on inner radius to rigid shaft rotating with constant angular velocity ω around its y axis. According to the derivation presented in Rao (1989) the disk can be discretized in the rotating $x\ y\ z$ coordinate system using linear isoparametric hexahedral finite elements (Šašek et al., (2006)). The equation of motion can be written in a configuration space defined by the vector

$$\boldsymbol{q}_D = \left[\ldots, u_j^{(F)}, v_j^{(F)}, w_j^{(F)}, \ldots, u_j^{(C)}, v_j^{(C)}, w_j^{(C)}, \ldots\right]_D^T \in \mathcal{R}^{n_D} \tag{18}$$

of nodal j displacements (see fig. 6) in direction of rotating axis $x,\ y,\ z$. The disk nodes are classified into free nodes (superscript F) and coupled nodes (superscript C) on the outer and inner surface of the blade roots. The mathematical model of the disk was derived in Šašek et al., (2006) using Lagrange's equations in the form

$$\boldsymbol{M}_D\ddot{\boldsymbol{q}}_D(t) + \omega\boldsymbol{G}_D\dot{\boldsymbol{q}}_D(t) + \left(\boldsymbol{K}_{sD} - \omega^2\boldsymbol{K}_{dD}\right)\boldsymbol{q}_D(t) = \omega^2\boldsymbol{f}_D\,, \tag{19}$$

where $\boldsymbol{M}_D$, $\boldsymbol{K}_{sD}$ and $\boldsymbol{K}_{dD}$ are symmetric mass, static stiffness and dynamic softening matrices, skew-symmetric matrix $\omega\boldsymbol{G}_D$ expresses gyroscopic effects and $\omega^2\boldsymbol{f}_D$ is force vector of centrifugal load.

The vector of generalized coordinates of the disk can be partitioned according to (18) as

$$\boldsymbol{q}_D = \begin{bmatrix} \boldsymbol{q}_D^{(F)} \\ \boldsymbol{q}_D^{(C)} \end{bmatrix},\ \boldsymbol{q}_D^{(F)} \in \mathcal{R}^{n_D^{(F)}},\ \boldsymbol{q}_D^{(C)} \in \mathcal{R}^{n_D^{(C)}}. \tag{20}$$

The displacements of the coupled disk nodes on condition of rigid blade roots modelled as a disk part can be expressed by displacements of referential nodes R_i which are identical with the first blade nodes $j = 1$ at blade roots (see fig. 6). This relation between coupled disk

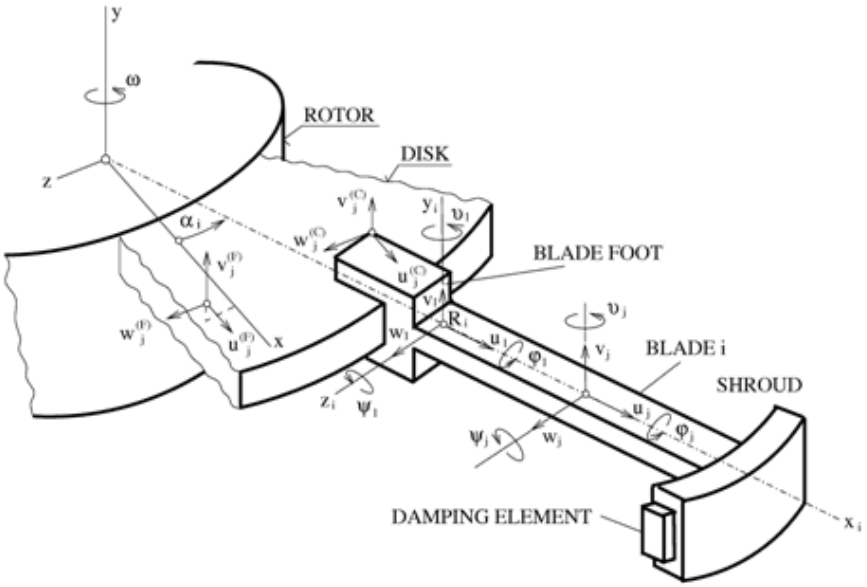

Figure 6: Scheme of bladed disk model.

displacements corresponding to blade i and blade displacements in referential node R_i is

$$\begin{bmatrix} u_j^{(C)} \\ v_j^{(C)} \\ w_j^{(C)} \end{bmatrix} = \begin{bmatrix} \cos\alpha_i & 0 & \sin\alpha_i \\ 0 & 1 & 0 \\ -\sin\alpha_i & 0 & \cos\alpha_i \end{bmatrix} \left[\begin{array}{ccc|ccc} 1 & 0 & 0 & 0 & z_j & -y_j \\ 0 & 1 & 0 & -z_j & 0 & x_j \\ 0 & 0 & 1 & y_j & -x_j & 0 \end{array}\right] \begin{bmatrix} u_1 \\ v_1 \\ w_1 \\ \varphi_1 \\ \vartheta_1 \\ \psi_1 \end{bmatrix}_{B,i}, \tag{21}$$

or shortly

$$\boldsymbol{q}_j^{(C)} = \boldsymbol{T}_{\alpha_i} \boldsymbol{T}_j \boldsymbol{q}_{1,i}, \qquad i = 1, 2, \ldots, r, \tag{22}$$

where x_j, y_j, z_j are coordinates of the coupled disk node j on the rigid blade foots in coordinate system x_i, y_i, z_i of the blade i with the origin in the first blade node and α_i is the angle between the rotating disk axis x and the rotating blade axis x_i. Coordinates of vector $\boldsymbol{q}_{1,i}$ express the referential node displacements in direction of blade rotating axes x_i, y_i, z_i and small turn angles of the blade cross section in node R_i.

The complete transformation between displacements of coupled nodes of the disk on the

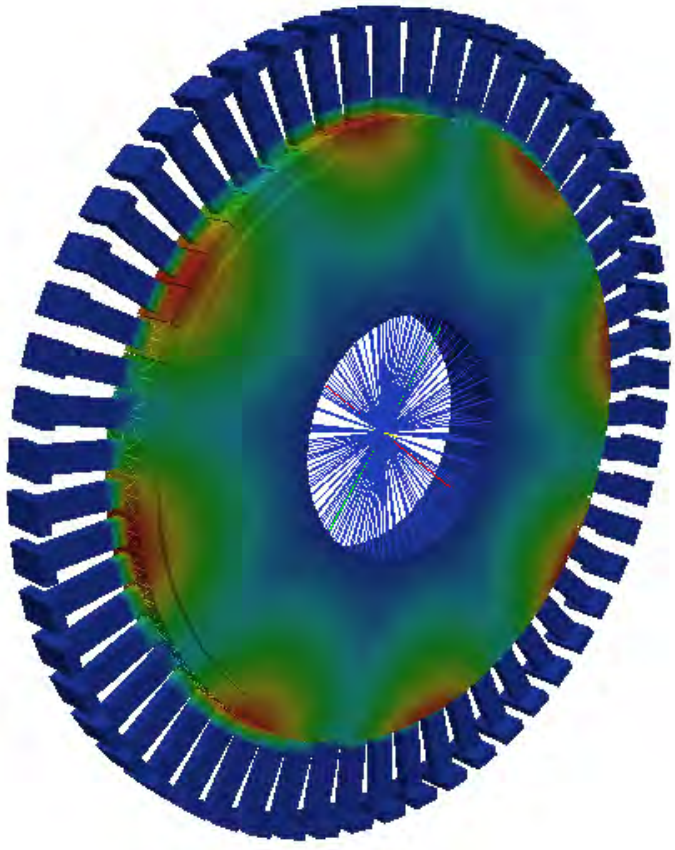

Figure 7: Mode shape of disk modelled with roots, without blade influence.

blade foots and the referential nodes R_i of all blades can be expressed in the matrix form

$$\begin{bmatrix} \vdots \\ \hline \boldsymbol{q}_j^{(C)} \\ \hline \vdots \end{bmatrix} = \begin{bmatrix} & \vdots & \\ \hline \dots & \boldsymbol{T}_{\alpha_i}\boldsymbol{T}_j & \dots \\ \hline & \vdots & \end{bmatrix} \begin{bmatrix} \vdots \\ \hline \boldsymbol{q}_{1,i} \\ \hline \vdots \end{bmatrix} \Rightarrow \boldsymbol{q}_D^{(C)} = \boldsymbol{T}_{D,R}\boldsymbol{q}_R. \tag{23}$$

The global transformation rectangular matrix $\boldsymbol{T}_{D,R} \in \mathcal{R}^{n_D^{(C)},n_R}$ describes the linkage between the disk (D) and the blade rim (R).

For illustration we present in tab. 2 some number of lowest natural frequencies of the nonrotating centrally clamped modeled disk (see fig. 7) with rigid blade foots but without blades. The nodes which lie on the inner radius are fixed in all directions. The mode shapes corresponding to natural frequencies are characterized by the number of nodal diameters (ND) and the number of nodal circles (NC). The modal values of the disk with foots modelled as flexible differ from the disk model with rigid foots very small Zeman et al., (2009). The natural frequencies of blade rim fixed on root diameter and the frequencies of full bladed disk are in tab. .

Table 2: Modal analysis of the disk, blade rim, bladed disk and the influence of disk condensation level.

Influence of disk condesantion level on natural frequencies [Hz] - free standing blades					
Mode shape	**Only disk with roots**	**Blade rim without disk**	**Full model - 13000 DOF**	**Condesation of disk - 320 DOF**	**Condesation of disk - 160 DOF**
1F 1ND	1711	418.28	404.97	405.00	405.61
1F 0ND	1682	418.28	405.43	405.50	405.14
1F 2ND	1832	418.28	406.28	406.35	406.51
1F 3ND	2555	418.28	410.70	410.77	410.93
1F 4ND	3802	418.28	413.64	413.71	413.86
1F 5ND	3806	418.28	415.06	415.12	415.26
1F 6ND	5352	418.28	415.86	415.87	415.99
1F 28ND	16280	418.28	417.58	417.58	417.72
2F 0ND	2890	840.93	813.81	813.81	813.86
2F 1ND	4400	840.93	851.85	821.88	824.52
2F 3ND	6844	840.93	821.92	821.94	828.43
2F 3ND	8566	840.93	822.05	822.14	828.64
3F 0NF	8085	1415.40	1413.23	1413.29	1413.57
3F 1ND	8312	1415.40	1410.35	1410.39	1410.66
3F 2ND	9011	1415.40	1408.47	1408.50	1408.78
3F 3ND	10196	1415.40	1411.98	1410.83	1411.11

8. The modelling of condensed bladed disk with friction elements in blade shroud

The motion equations of the fictive undamped system assembled from uncoupled subsystems – the central clamped disk with/without rigid blade roots and blade rim with friction elements in

shroud – in the configuration space

$$\boldsymbol{q} = \left[\left(\boldsymbol{q}_D^{(F)} \right)^T \left(\boldsymbol{q}_D^{(C)} \right)^T \boldsymbol{q}_R^T \right]^T \tag{24}$$

can be formally rewritten as

$$\boldsymbol{M}\ddot{\boldsymbol{q}}(t) + \omega \boldsymbol{G}\dot{\boldsymbol{q}}(t) + \left(\boldsymbol{K}_s + \omega^2 \boldsymbol{K}_\omega - \omega^2 \boldsymbol{K}_d \right) \boldsymbol{q}(t) = \omega^2 \boldsymbol{f}. \tag{25}$$

According to mathematical models (19) and (14), all matrices have the block-diagonal form

$$\begin{gathered} \boldsymbol{X} = diag\left(\boldsymbol{X}_D,\ \boldsymbol{X}_R\right),\ \boldsymbol{X} = \boldsymbol{M},\ \boldsymbol{G},\ \boldsymbol{K}_d, \\ \boldsymbol{K}_s = diag(\boldsymbol{K}_{sD},\ \boldsymbol{K}_{sR} + \boldsymbol{K}_C^{(R)}),\ \boldsymbol{K}_\omega = diag(\boldsymbol{0},\ \boldsymbol{K}_{\omega R}) \end{gathered} \tag{26}$$

and $\boldsymbol{f} = \left[\boldsymbol{f}_D^T,\ \boldsymbol{f}_R^T\right]^T$. The vector of generalized coordinates $\boldsymbol{q}(t)$ of the real bladed disk in consequence of the couplings (23) can be transformed into new vector $\tilde{\boldsymbol{q}}$ in the form

$$\begin{bmatrix} \boldsymbol{q}_D^{(F)} \\ \boldsymbol{q}_D^{(C)} \\ \boldsymbol{q}_R \end{bmatrix} = \begin{bmatrix} \boldsymbol{E}_D^{(F)} & \boldsymbol{0} \\ \boldsymbol{0} & \boldsymbol{T}_{D,R} \\ \boldsymbol{0} & \boldsymbol{E}_R \end{bmatrix} \begin{bmatrix} \boldsymbol{q}_D^{(F)} \\ \boldsymbol{q}_R \end{bmatrix} \text{ or shortly } \boldsymbol{q} = \boldsymbol{T}_F \tilde{\boldsymbol{q}}. \tag{27}$$

The mathematical model of the central clamped bladed disk with friction elements in blade shroud in the configuration space $\tilde{\boldsymbol{q}}$ takes the form

$$\tilde{\boldsymbol{M}}\ddot{\tilde{\boldsymbol{q}}}(t) + \omega \tilde{\boldsymbol{G}}\dot{\tilde{\boldsymbol{q}}}(t) + \left(\tilde{\boldsymbol{K}}_s + \omega^2 \tilde{\boldsymbol{K}}_\omega - \omega^2 \tilde{\boldsymbol{K}}_d \right) \tilde{\boldsymbol{q}}(t) = \omega^2 \tilde{\boldsymbol{f}}, \tag{28}$$

where $\tilde{\boldsymbol{X}} = \boldsymbol{T}^T \boldsymbol{X} \boldsymbol{T},\ \boldsymbol{X} = \boldsymbol{M}, \boldsymbol{G}, \boldsymbol{K}_s, \boldsymbol{K}_d, \boldsymbol{K}_\omega$ and $\tilde{\boldsymbol{f}} = \boldsymbol{T}^T \boldsymbol{f}$.

The number of free node elastic coordinates $\boldsymbol{q}_D^{(F)}$ of the disk is very large for future dynamic analysis of the bladed disk with dry friction elements. Hence, disk DOF number corresponding to free node coordinates and blades DOF number is desirable to reduce by use of the modal condensation Slavík et al., (1997). Let modal properties of the conservative model of the non-rotating disk with blade roots isolated from blades in cross-sections passing through referential nodes be characterized by spectral and modal matrices. These matrices satisfy the orthogonality and norm conditions

$$\boldsymbol{V}_D^T \boldsymbol{M}_D \boldsymbol{V}_D = \boldsymbol{E}, \qquad \boldsymbol{V}_D^T \boldsymbol{K}_D \boldsymbol{V}_D = \boldsymbol{\Lambda}_D, \tag{29}$$

where $\boldsymbol{E}$ is unit matrix. The modal matrix of the disk can be rearranged into the block form

$$\boldsymbol{V}_D = \begin{bmatrix} {}^m\boldsymbol{V}_D^F & {}^s\boldsymbol{V}_D^F \\ {}^m\boldsymbol{V}_D^C & {}^s\boldsymbol{V}_D^C \end{bmatrix} \tag{30}$$

corresponding to decomposition (20) and eigenvectors are separated into frequency lower eigenvectors (so called master - superscript m) and frequency higher eigenvectors (so called slave - superscript s). The vector $\boldsymbol{q}_D(F)$, corresponding to free disk nodes, can be approximately transformed in the form

$$\boldsymbol{q}_D^{(F)} =^m \boldsymbol{V}_D^{(F)} \boldsymbol{x} \tag{31}$$

where ${}^m\boldsymbol{V}_D^{(F)}$ is the modal submatrix corresponding to free disk displacements and frequency lower eigenmodes. Higher natural modes usually contribute less to the disk deformation and

their influence can be neglected. The vectors $\boldsymbol{q}_B$, corresponding to blade displacements, can be transformed by same way as the disk.

The vector $\boldsymbol{q}$ of the fictive system in consequence of the coupling (23) and modal transformations (31) (and blade rim by same way) can be transformed into new vector $[\boldsymbol{x}_D^T \quad \boldsymbol{x}_R^T]^T$ of the dimension $m = m_D + r.m_B$. The transformation is given by

$$\begin{bmatrix} \boldsymbol{q}_D^{(F)} \\ \boldsymbol{q}_D^{(C)} \\ \boldsymbol{q}_R \end{bmatrix} = \begin{bmatrix} {}^m\boldsymbol{V}_D^{(F)} & \boldsymbol{0} \\ \boldsymbol{0} & \boldsymbol{T}_{D,R}^m \boldsymbol{V}_R \\ \boldsymbol{0} & {}^m\boldsymbol{V}_R \end{bmatrix} \begin{bmatrix} \boldsymbol{x}_D \\ \boldsymbol{x}_R \end{bmatrix} \qquad \text{or shortly} \qquad \boldsymbol{q} = \boldsymbol{T}\boldsymbol{x} \quad , \tag{32}$$

where matrix ${}^m\boldsymbol{V}_R = diag({}^m\boldsymbol{V}_B \in R^{n_R, m_R}$ and $m_R = r.m_B$. Details of this condensation can be seen in Zeman et al., (2009).

The condensed mathematical model of the bladed disk after elimination of the coupled displacements takes the form

$$\tilde{\boldsymbol{M}}\ddot{\boldsymbol{x}}(t) + \omega\tilde{\boldsymbol{G}}\dot{\boldsymbol{x}}(t) + \left(\tilde{\boldsymbol{K}}_s - \omega^2\tilde{\boldsymbol{K}}_d + \omega^2\tilde{\boldsymbol{K}}_{\omega^2}\right)\boldsymbol{x}(t) = \omega^2\tilde{\boldsymbol{f}}\,, \tag{33}$$

where transformed matrices are

$$\tilde{\boldsymbol{X}} = \boldsymbol{T}^T\,\boldsymbol{X}\,\boldsymbol{T}, \qquad \boldsymbol{X} = \boldsymbol{M},\,\boldsymbol{G},\,\boldsymbol{K}_s,\,\boldsymbol{K}_d,\,\boldsymbol{K}_\omega, \quad \tilde{\boldsymbol{f}} = \boldsymbol{T}\boldsymbol{f}. \tag{34}$$

The condensed model (33) has much lower DOF number compared to noncondensed (full) model gained from the fictive model by the transformation (32) with the modified transformation matrix $\boldsymbol{T}_F$. This matrix originates from $\boldsymbol{T}$ by the change of the modal submatrix ${}^m\boldsymbol{V}_D^{(F)}$ of the disk and the block diagonal matrix ${}^m\boldsymbol{V}_R$ for the unit matrices $\boldsymbol{E}_D$ of order $n_D^{(F)}$ and $\boldsymbol{E}_R$ of order n_R.

9. Measurement of rotating bladed disk

The next step after identifying the damping ratio of beams leads to identification of the damping ratio for free standing blades under rotation. Rotation is a very important aspect for this measurement. Due to the rotation, the centrifugal forces are generated. It retunes the blades - frequencies are changing (make stiffness higher) and also it fixes the blade root in the grooves in the disc. Even more if the blades have friction elements between shrouds, the contact areas are changing. This determined the boundary conditions of measurement.

It is evident that damping of such blades cannot be calculated and results obtained without rotation cannot be applied on blades under rotation. First type of blades was free standing blades. This test was carried out to compare damping ratio with and without rotation and to be compared with measurement realized at the beams. In the second case, the same blades were used but the friction dampers were added. For dynamic measurements under rotation, vacuum high speed stand was constructed in Doosan Skoda Power.

- Maximum speed 12 000RPM
- Vacuum up to 3mBar
- Maximum diameter of bladed disk 1.2m

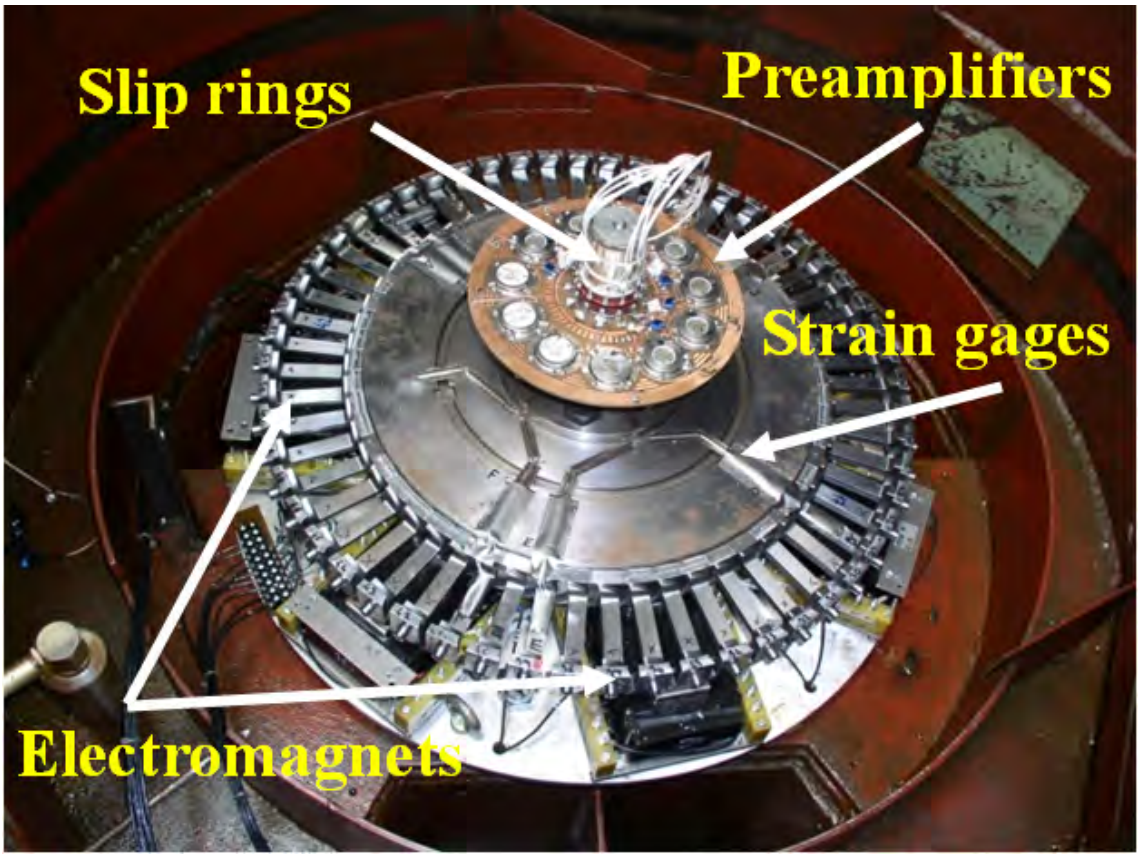

Figure 8: Photo of high speed stand (bladed disk, electromagnets, preamplifiers, transmission slip rings.

- Excitation systems - permanent magnets, electromagnets, air jet, water jets

In order to enable dynamic excitation the stand was equipped by a set of alternate electromagnets placed on the duraluminum plates. Boards with 7 electromagnets were placed above and below the blades in the middle distance of 7 mm. This distance was chosen to provide the highest power possible with respect to security. Fig. 8 shows us the placement of bladed disk over one row of magnets. The figure also shows preamplifiers and transmission slip rings.

In order to determine damping ratio of blades, the blades had to be excited using electromagnetic sweep. The excitation had to be determined for each nodal diameter. Minimum excitation force of 5N was required for one magnet. In contrast with paper Jones and Cross, (2003), where permanent magnets were used, Doosan Škoda Power used for excitation sets of AC electromagnets in this case. There are more than 10 years of experience with AC electromagnets development and their usage for steam turbine blading. In comparison with permanent magnets AC electromagnets have lower force amplitude however the frequency of excitation can be controlled with higher accuracy. The main disadvantage of permanent magnet is induction of eddy currents which heat the structure very quickly that is why the material properties are changing. The largest advantage of AC electromagnet is that all measurement points including many frequencies and nodal diameters can be measured at nominal speed with one set of magnets. It is very important because the boundary conditions are stabilized (stiffness, blade untwist, normal forced to friction dampers). On the other hand it is very hard to control frequency and phase shift between electromagnets. Both had to respect following relationship (35). Of course the

circumferential positions of electromagnets have to be considered.

$$f_{excitation} = f_{natural} \pm N.f_{rotation} \tag{35}$$

This equation describes relation between excitation and natural frequency. When ND > 0, the excitation force is different from the natural frequency. It has positive influence to signal noise ratio.

The special algorithm was used to generate maximal excitation force from electromagnets (ECM). This algorithm involves physical properties of electromagnets (i.e. it can only attract the iron). It seems to be easy to excite by one pulse for concrete time when the blades goes around ECM. But the force from one EMC is for higher frequencies only about 5 N. That's why the algorithm generates signal for all EMCs during whole measurement and its dependent on required nodal diameter. The frequency of EMC signal is then faster then the natural frequency, as in (35). This is drawn on fig. 9. The locations of three first EMC are expressed by black, green and red vertical line. The curves with same color represents the force generated by these EMCs. The dark blue curve represents blade vibration in time - this excitation is ideal for excite the blade with disk and with required number of nodal diameters. When the blade goes around EMCs, the relative amplitude EMC force/blade is same as derivation (positive or negative).

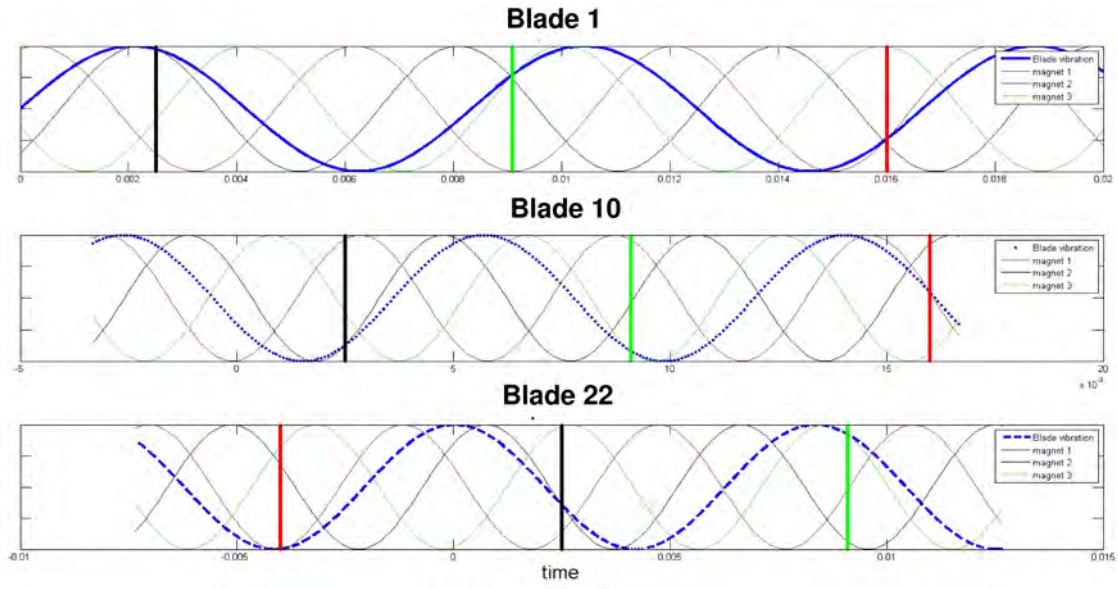

Figure 9: Effect force from electromagnets to blades.

To detect damping using half power point method the excitation frequency had to vary around the resonance. Fourier amplitude spectrum close to the resonance results from this type of frequency sweep.

The damping ratio dependence on the blade vibration amplitude is shown in fig. 10. The values of damping ratio were identified for 4 natural frequencies. These frequencies belong to the first mode shape of the 2^{nd} to the 5^{th} nodal diameter of the running wheel (rotation speed 3000 RPM) where 6 strain gages were used for this measurement. Particular values of damping ratio are approximated by the regression line that shows the increase of damping ratio with the amplitude of blade oscillation. The significant variance of damping ratio is evident in the fig. 10. This discrepancy is caused by two factors. The first factor is that different blade with

slightly different manufacturing is measured that means different boundary condition. Secondly when mistuning occurs there is an error during evaluation because there are two close interacting peaks in frequency spectrum. The damping ratio comparison of beams and blades under rotation is shown in fig. 4. It is apparent from this figure that the damping ratio of free standing blades under rotation is a little bit higher than the damping ratio of beams. This is caused by additional construction damping in blade root attachment.

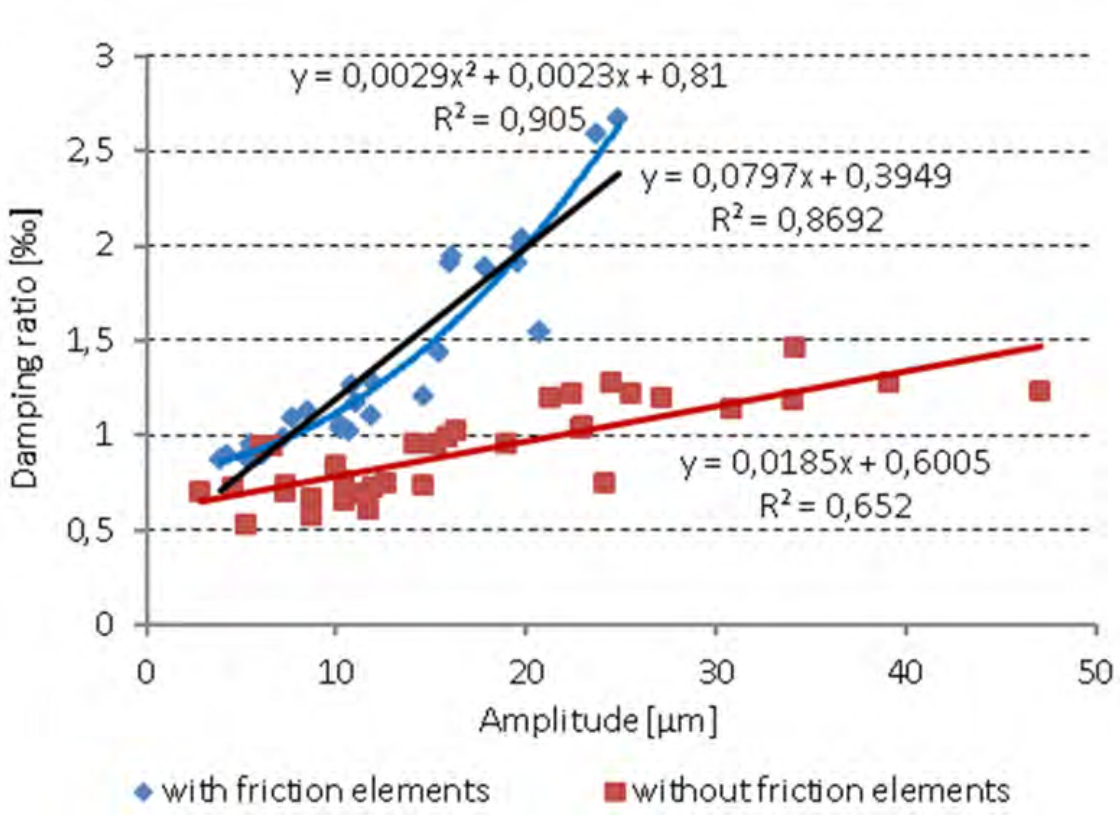

Figure 10: Damping ratio dependence on blade vibration amplitude and comparison of free standing and shrouded blades with friction elements.

As mentioned above the first measurement was done with original steam turbine blades in vacuum chamber in Doosan Škoda Power. But the force from EMC was much lower than expected - only 5 N for this type of material, which has relatively low permeability. That was the reason for change of blade profile - the aerodynamic airfoil was changed to rectangular shape 16x8 mm. This change results in lower frequencies and in lower stiffness of blade. Moreover, the frequencies are close to natural frequencies of specimens for damping material measurement, as mentioned above.

It is evident from fig. 10 that the coupled blades with friction elements have higher damping ratio than the free standing blades. But this diagram does not show whether nodal diameters influence the size of damping ratio or not. The influence of different nodal diameters will be presented in next paper.

10. Comparison of measurement and FE models

In this section, the modal properties of FE model created in MATLAB (and condensed) is compare with reference detailed model in ANSYS and with measurement. The fig. 11 shows natural frequencies for bladed disk with free standing blades. The small difference between measured and computed values is not significant and it can be assumed that there will be no problem with damping parameter identification in mathematical model. The correlation can be done by change of elastic modulus.

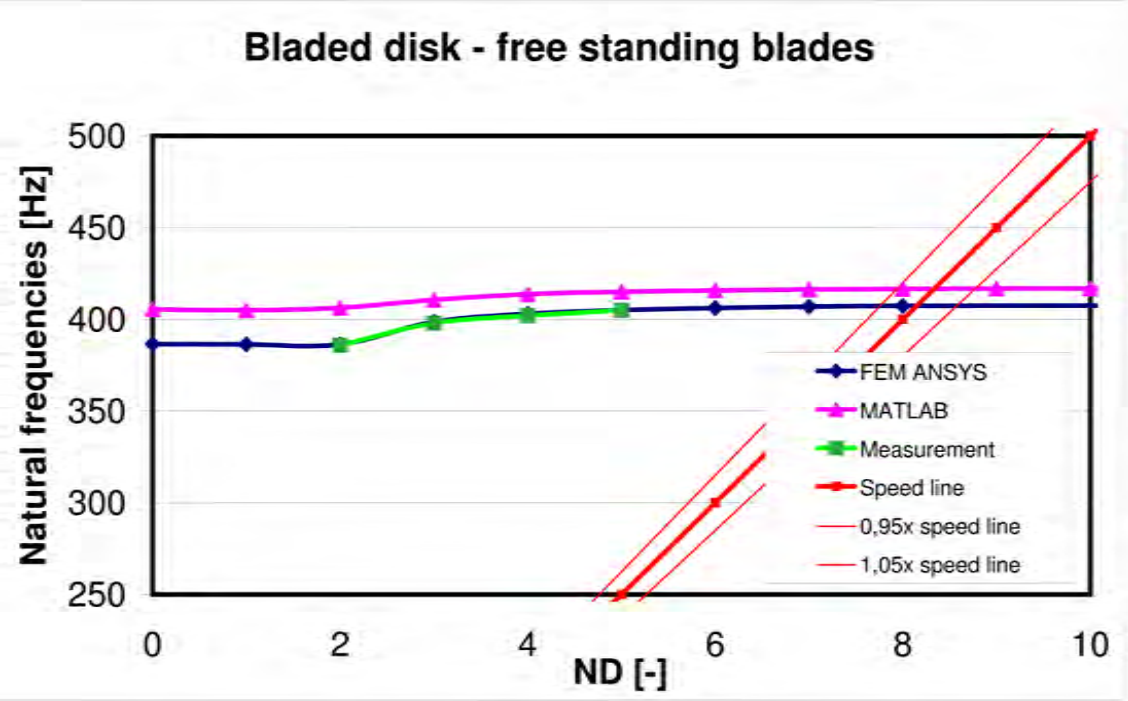

Figure 11: SAFE diagram for natural frequencies of bladed disk with free standing blades - measurement and FE results.

Although the correlation between modal properties FE models and measurement for free standing blades is very good, there is high error for bladed disk with friction elements, see fog. 12. The first measured frequency is close to computed values, But the difference measurement - FE models rises with higher nodal diameters. But it can be seen the stiffening of the bladed disk with friction elements compare to freestanding blades (in fig. 12 the free standing blades are drawn by dashed line). In fig. 11 there is possible resonance with multiples of harmonics for 7^{th} and 8^{th} nodal diameters, where the safety requirement is 5% difference between natural frequency and possible excitation frequency.

The disagreement between measured and calculated natural frequencies in fig. 12 can be caused by sliding contact areas between shrouds and friction elements. Higher excited nodal diameter, less blades are in one sinusoidal. That cause higher relative displacements between adjacent shrouds and that can caused sliding. The introduced methodology will be updated to involve this phenomena. One way can be by identification of contact parameters in section 5.

The results obtained by measurement for different nodal diameters will be used for testing methodology. It will be included in amplitude-frequency diagrams from harmonic excitation. The excitation can be simulated only as harmonic in contrast to another type of excitation. The

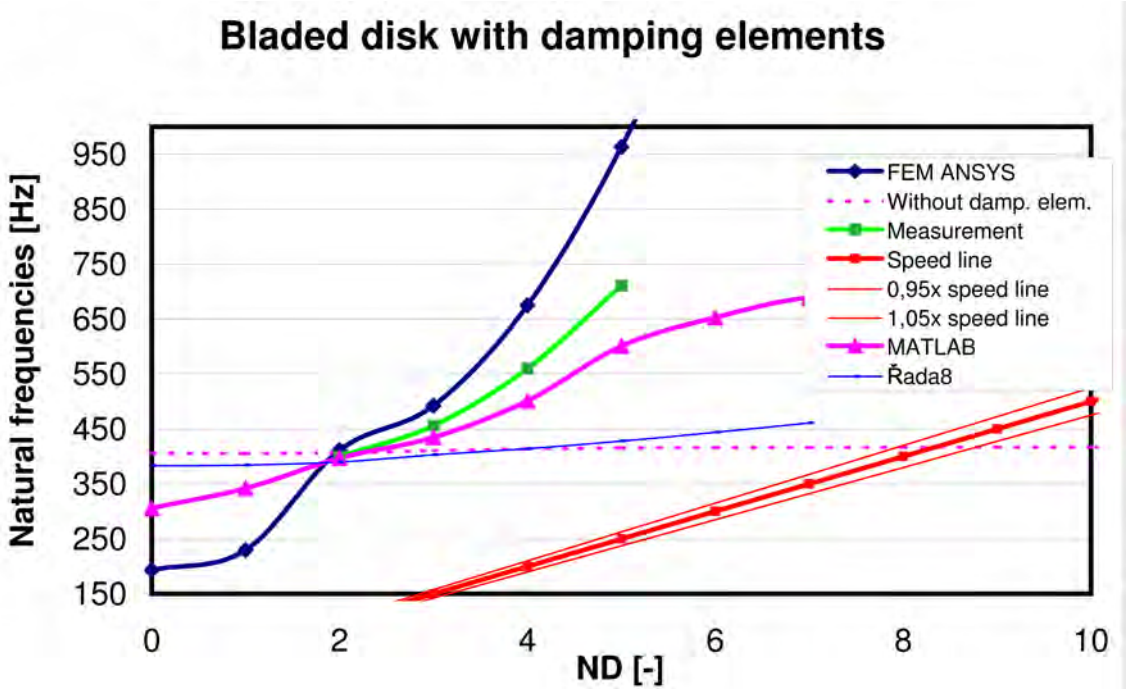

Figure 12: SAFE diagram for natural frequencies of bladed disk with friction elements - measurement and FE results.

purpose is in section 9 - the excitation from EMCs is sinusoidal. Other type of excitation, i.e. water jet, air-jet, permanent magnets, results in poly-harmonical excitation, which should be described by Dirac pulse and by Fourier row. That can result in mistuning response which leads to non-clearly conclusions.

11. Conclusions

This paper summarizes the measurements done to the bladed disk with and without friction elements. The measurement includes material damping, damping of blade-root connection and the damping caused be friction element motion on several mode shapes.

The detailed methodology for model creating is introduced and compared with real data and with commercial software. This methodology allows fast model computation. The modal condensation of model is prepared to identification and optimization of friction element parameters. The correctness of the blade model was verified by measurement in hydraulic press. For bladed disk with free standing blades there is very good agreement with measured data, but for bladed disk with friction elements there is higher disagreement for both FE models as well as measurement. The methodology enables the identification of contact and damping parameters and the model can be tuned for real measured data.

Although the measurement was successful more excitation sources will be used. The reason is to identify more natural frequencies and to identify damping for higher nodal diameters. That will be done with system of water-jets simulating the stationary blades. This will be useful for model testing but there will be the need of real force distribution modelling, as discussed above. The measurement can be used for analysis of friction element properties, such as for investigation of sprayed contact surfaces impact. This sprayed contact surfaces can have lower friction coefficient which can lead to higher relative motion of the friction element between shrouds.

In next paper, the forced response of mathematical model and experimental data will be compare and the parametric optimization of the friction element will be applied to the bladed disk after identification.

12. Acknowledgment

This work was supported by the GA CR project No. 101/09/1166 ”Research of dynamic behaviour and optimization of complex rotating systems with non-linear couplings and high damping materials”.

13. References

Šašek, J., Zeman, V. & Hajžman, M. 2006: Modal properties of rotating disks, in *Proceedings of the 22nd Computational Mechanicss 2006* (J. Vimmr ed.), Nečtiny, pp. 593-600.

Kellner, J. & Zeman, V. 2006: Infuences of dynamic stiffnes, centrifugal forces and blade's elastic seating on blade modal properties, *Proceedings of the 8th Applied Mechanics* , pp. 47-48.

Zeman, V., Šašek, J. & Byrtus, M. (2009): Modelling of rotating disk vibration with fixed blades. *Modelling and optimization of physical systems, 8* , Gliwice, pp125-130.

Rao, S., S. (1989): *The finite element method of engineering*. Pergamon Press, Oxford.

Kellner, J. (2009): *Vibration of turbine blades and bladed disks (in Czech)*, Doctoral thesis, UWB, Pilsen.

Riwin, E., I. (1999): *Stiffness and damping in mechanical design*.Marcel Dekker, Inc., New York.

Kubin, Z., Polreich, V., Černý, V., Babková, P. & Prchlík, L. (2013): Damping identification and its comparison for various types of blades couplings, in: *Proceedings of ASME Turbo Expo 2013*, GT2013- 95438.

Slavík, J., Stejskal, V. & Zeman, V. (1997): *Základy dynamiky stroju.* ČVUT, Praha.

Jones, K. W. & Cross, C. J., (2003): Traveling Wave Excitation System for Bladed Disks. *Journal of Propulsion and Power*, Vol. 19, No. 1.

Kellner, J., Zeman, V. & Šašek, J. (2010): Modelling of bladed disk with damping effects in slip surfaces of shroud. In: *Proceedings of the Ingineering mechanics 2010* (I. Zolotarev ed.), Inst. of Thermomechanics, AS CR, Prague, pp. 59-60.

Hajžman, M., Bruha, J., Zeman, V., Pešek, L. & Rychecký, D. 2013: Basic Optimization Methodology for the Design of Friction Damping in Blade Shrouds. *ASME 2013 International Design Engineering Technical Conferences (IDETC)*, August 4-7, 2013 in Portland, Paper number DETC2013-13443.